Chemical Science

Accepted Manuscript

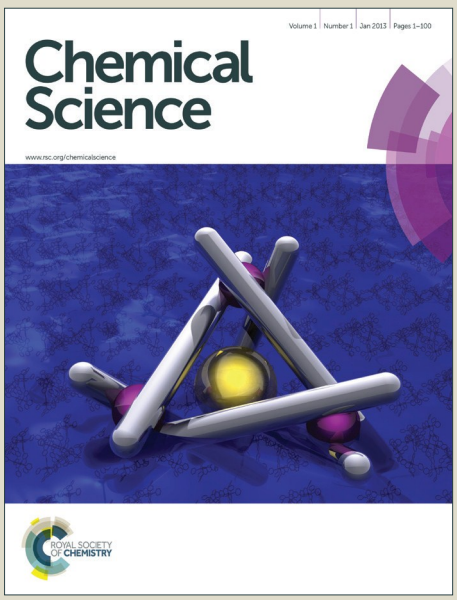

ROYAL SOCIETY OF CHEMISTRY

www.rsc.org/chemicalscience

Chemical Science

RSCPublishing

ARTICLE

Novel design of porphyrin based D-s-A systems as molecular rectifiers

Cite this: DOI: 10.1039/x0xx00000x

Kavita Garg,[a*] Chiranjib Majumder,[b] Shiv K. Gupta,[c] Dinesh Kumar Aswal,[c] Sandip Kumar Nayak,[a] and Subrata Chattopadhyay[a]

Received 00th January 2012,
Accepted 00th January 2012

DOI: 10.1039/x0xx00000x

www.rsc.org/

Two Si-based hybrid self-assembled monolayers of porphyrin based on D-s-A system were synthesized by electro-grafting. The monolayers showed a stable and reversible rectification at room temperature. The monolayer, fabricated using the porphyrin with an eleven-carbon alkyl chain linker was comparatively more compact and showed a 10^5 times high rectification ratio (RR) relative to the other similar system having a six-carbon alkyl chain linker, possibly because of compact packing.

Introduction

Miniaturization is the need of the electronic industry, but is limited by the change in bulk properties of materials as we go to nano dimensions. Most of the successes in this field have focused on the electrical properties of organic molecules placed between metal electrodes.[1–5] In particular, self-assembled monolayers (SAMs) of alkane and aromatic thiols on gold substrates have been very popular to construct the metal-molecule-metal (MMM) junctions.[6–10] Concurrently, efforts on synthesizing metal-molecule-semiconductor (MMS) junctions by covalent linking of organic molecules to semiconductor surfaces are gaining momentam.[11] Such assemblies present opportunities for novel molecular electronic charge transport mechanisms, and are potentially compatible with the conventional metal oxide–semiconductor (MOS) technology. To this end, there is a burgeoning interest in small organic molecules, capable of switching their redox status, as in association with semi-conductors such as Si, these may scale down the size of the molecular electronic devices.[12–14] Here, the surface potential tailoring can be achieved by chemically-grafted organic molecules on Si to develop improved hybrid molecular devices. For example, the p-n junction threshold voltage for rectification can be adjusted by changing the electronic nature of the organic π group molecules, instead of the classical doping method.[14] Different techniques like Langmuir-Blodgett (LB) films,[15] or SAMs of organic molecules on solid substrates via MMM junctions[16] are most commonly used for this purpose. Compared to the LB films, the SAMs are easy to prepare and may be more robust as the organic molecules are sturdily anchored on the metal substrates at fixed distances. Chemically bonded monolayers on Si surfaces can be prepared either on Si oxide (SiOx) surfaces or on oxide-free Si,[11,17] the latter being preferred due to better Si−molecule electronic coupling and lack of charging effect. In-depth reviews with excellent analysis of different methods of fabrication and characterization of SAM junctions on H-terminated Si surfaces are available.[18,19] The usually-adopted protocol for constructing densely packed Si-organic hybrids involve deposition of some functionalized alkenes/alkynes, using heat,[20] light,[21,22] electrochemical techniques, radical initiators,[23] or Lewis acids,[24] as well as with alkylhalides via a Grignard route or lithiation.[25] This is followed by attachment of the electro-active organic molecules at the terminal functionality of the resultant alkane/alkene-Si hybrids by esterification or amidation. However, due to steric factor, all the deposited alkane/alkene moieties can't be modified with the organic molecules. This may produce non-uniform organic-Si hybrids. During our previous work, we found that cathodic electro-grafting of the pre-synthesized alkenylated electro-active organic molecules on Si-H surfaces can conveniently provide the SAM-based molecular electronics devices, with the following advantages.[26] The process is simple; can be monitored online to ensure completion of deposition; can exclude oxidation and/or hydrolysis at the Si surfaces due to the negative potential bias on the Si wafers; and produce the materials where the Si-H surfaces are modified only by the chosen molecules.

Amongst the electron-rich organic molecules, porphyrins[27] are ideally suited for fabricating molecular devices because they (i) form stable π-cation radicals, and exhibit two accessible cationic states in monomeric forms;[28–32] (ii) have long charge retention times, contributing to less power consumption; (iii) are highly stable,[33] and (iv) can form self-assembled structures.[34] In view of these favourable attributes, porphyrins have been extensively used as the π molecules to construct storage devices, molecular wires and memory devices. Reports on current rectification by C60-porphyrins combinations also exist.[35] Molecules, showing rectification behavior with high rectification ratio (RR) is very useful for making diodes. According to Aviram and Ratner, a single molecule with donor-spacer-acceptor (D-s-A) structure would behave as a rectifying diode when placed between two electrodes, where the σ-bond bridge would prevent the direct overlap of the donor (D) and

acceptor (A) energy levels to allow unidirectional flow of current.[1] Several groups have experimentally verified this model, but porphyrins have never been used for this purpose in silicon hybrid systems.[36,37] In the present investigation, two such single molecules (**5a**/**5b**) were synthesized, where the porphyrin and aniline moieties served as the (A) and (D) units respectively, while a —CH_2-NH— moiety was anticipated to be the required spacer. These molecules were electro-grafted on the Si-surfaces using the C-6/C-11 alkenyl chain of **5a**/**5b** as the linker to construct the respective MMS heterostructures. Results of their *I-V* behavior revealed high current RRs by these assemblies. Moreover, a subtle change in the linker length significantly changed the monolayer packing on the Si-surfaces, resulting in a pronounced alteration in the current rectification property.

Results and discussion

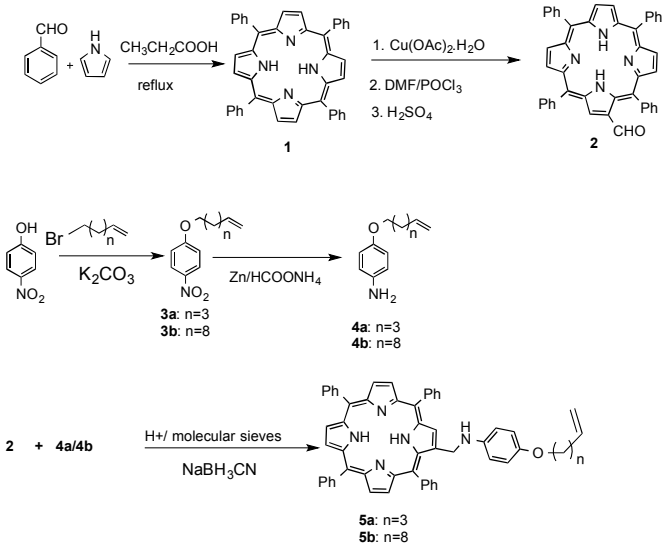

Scheme 1. Synthesis of the D-s-A molecules **5a** and **5b**

Synthesis of the porphyrins

The porphyrin-based functional molecules are by and large synthesized by functionalization at the aryl moieties of unsymmetrical *meso*-tetraryl porphyrins. However, synthesis of the unsymmetrical porphyrins is fraught with limitations such as poor yields and tedious isolation procedures. Instead, functionalization at the pyrrol units of the porphyrins offers a better alternative to alter the porphyrin scaffold. Nevertheless, this strategy is rarely used, because the porphyrin pyrrol units are inert towards most of the electrophilic reactions like Friedal-Craft alkylation and acylation, while their halogenation[38] and nitration[38,39] often lead to di- or higher substituted products. In exception to these, the Vilsmeir-Haack reaction can provide the mono-formyl porphyrins in appreciable yields.[39] We reasoned that the formyl group can subsequently be used to construct the desired D-s-A structure for the present studies. Thus, following Bonfantini's method,[39] tetraphenylporphyrin (TPP, **1**) was converted to Cu(II)-TPP, and subjected to the Vilsmeir-Haack reaction to obtain the β-formyl-TPP (**2**). For the synthesis of the donor part, *p*-nitrophenol was *O*-alkylated with 1-bromohexene or 1-bromo-10-undecene to furnish the compounds **3a** and **3b** respectively. These were converted to the aniline derivatives **4a** and **4b** by reduction with Zn/HCO_2NH_4. Next the aldehyde **2** was separately subjected to reductive amination using **4a** and **4b** to obtain the target porphyrins **5a** and **5b** respectively. Earlier Welch *et al*.[40] synthesized the Schiff's base of **2** in 72 h in toluene using a Dean-Stark apparatus for simultaneous removal of water. We performed the reductive amination in THF in the presence of molecular sieves 4Å followed by a one-pot reduction of the intermediate imine to obtain **5a** and **5b** in improved yields (~78%) in only 6 h.

Device fabrication

PREPARATION OF THE SI-HYBRIDS

The molecules **5a** and **5b** were electrochemically deposited on H-terminated silicon via a possible two-steps process, schematically shown in the supplementary materials (**Fig. SL1.**). In the first step, application of a negative potential to the working electrode releases H free radicals from Si-H surfaces. The newly generated nucleophilic Si atoms subsequently react with the alkene function of **5a** and **5b** to form the Si-C bond, resulting in the irreversible oxidation peak at ~ 0.3 V. A similar oxidation peak was observed with 1-undecene (**Fig. SL2.**), but not with the blank (only electrolyte), confirming our interpretation. The cyclic voltammograms (CVs) (**Fig. 1**), recorded during this electrochemical deposition helped to monitor the extent of deposition. Disappearance of the oxidation peak indicated completion of the process. The AFM analyses revealed the formation of homogeneous monolayers with both **5a** and **5b** at 25 scans.

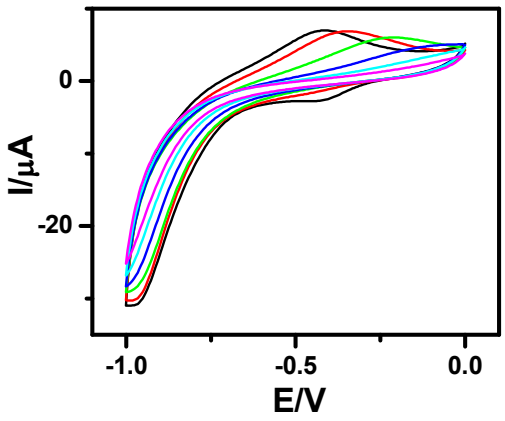

Fig. 1. CVs indicating electrografting of **5b** molecules on Si (n++) wafers. The deposition was carried out by CV at a scan rate of 0.05 V/s under N_2 atmosphere using Si wafers as the WE, Pt as the CE, Ag/AgCl as the RE, and 0.1 M Bu_4NP as the electrolyte, using **5b** (1 μM) in dry CH_2Cl_2.

CHARACTERIZATION OF THE MONOLAYERS

To ensure the monolayer deposition on Si, the electro-grafted materials were characterized by contact angle measurement, polarized FT-IR spectroscopy, ellipsometry, AFM, secondary ion mass spectrometry (SIMS) and electrochemistry. The contact angles of deionized water at the Si surface, grafted with **5a** and **5b** were 55° and 64° respectively. For the cleaned Si wafer and the C-11 alkyl-grafted Si surfaces, these were 84° and 112° respectively. The value for the the cleaned Si wafer is consistent with several previous reports.[41–45] The low contact angles of the porphyrin monolayers suggested them to be tilted on the Si-surface, exposing the pyrrole and amine nitrogen atoms to interact with water droplets. The observed contact angles of the porphyrin monolayers are in close proximity with the reported contact values (66-74°) for the thiophene-

terminated alkyl monolayers on Si-surfaces that were prepared by a late-stage attachment of the aryl moieties.[46] This established the suitability of our direct attachment protocol for the preparation of the monolayers. The average thicknesses of the monolayers, estimated by ellipsometry were found to be 2.4±0.1 nm and 2.9±0.2 nm in case of **5a** and **5b** respectively. The AFM analyses revealed that the monolayers, formed at 25 scans were organized with least number of voids and hillocks. The void depth and rms roughness for the **5a** monolayers were ~ 2.5 nm and 0.91 nm, while that for **5b** were 3 nm and 0.7 nm respectively (**Fig. 2**). Compared to **5a**, the monolayers of **5b** were more compact and uniform with larger grain size.

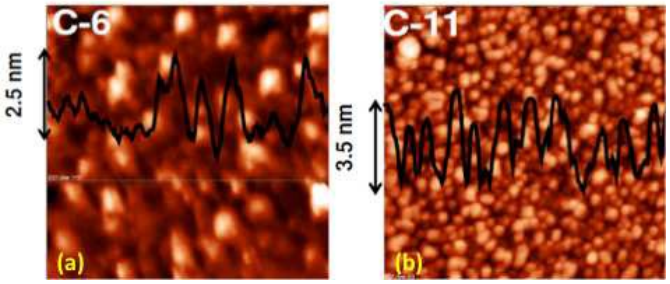

Fig. 2 AFM images of (2 μm × 2 μm) (a) **5a** and (b) **5b** monolayers on Si (111).

The fast scan (10 V/s) CVs (**Fig. 3**) of the respective porphyrin monolayers exhibited a reversible peak at +0.8 V, confirming attachment of the porphyrin moiety. This was absent in the blank Si samples and the C-11 alkyl monolayers. The net charge transferred during the oxidation process, calculated from the areas under the oxidation peak divided by the scan rate were 8.6×10^{-7} C and 2.45×10^{-6} C respectively for **5a** and **5b**. From these, the surface coverages by the monolayers were calculated using the formula: surface coverage = total charge /(F× area dipped in electrolyte). The surface coverages were 1.11×10^{12} and 4.5×10^{14} molecules/cm^2 respectively for **5a** and **5b**. Thus, the areas occupied by each molecule in **5a** and **5b** monolayers were 90 nm^2 and 22 Å^2 respectively, indicating that **5b** formed more compact monolayers than **5a**. The significantly higher value with **5a** compared to that reported[19] for the monolayers of simple C_{18}-, C_{16}-, and C_{12}- alkanes on Si (100) revealed poor packing. This may be due to the edge-on orientations of the porphyrins.[47] On the other hand, the value with the **5b** monolayers matched well with the theoretically calculated diameter (14.8 Å) of TPP,[48] and indicated that they are tightly packed by π–π stacking, as also revealed by the AFM image (**Fig. 2**). Consistent with the AFM analyses, the surface covered by **5b** was several fold that by **5a**.

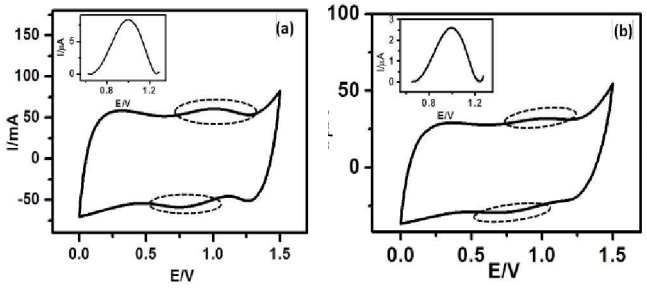

Fig. 3. Fast scan CVs for the monolayers of (a) **5a**; (b) **5b**, electro-grafted on Si (n++) wafers. The CVs were recorded under N_2 atmosphere at a scan rate of 10 V/s using the respective monolayer-grafted Si as the WE, Pt as the CE, Ag/AgCl as the RE, and 0.1 M Bu_4NP as the electrolyte. The circles indicate the reversible peaks. Insets show the magnified redox peaks, after background corrections.

The SIMS for the **5a** monolayers showed mass peaks at m/z 795, 691, 675 and 596 amu, while that for the **5b** monolayers appeared at m/z 777 and 386 amu (**Fig. 4**), revealing that the molecules remained intact during grafting process. The observed higher mass fragments in case of the C-11 monolayers was consistent with its longer alkyl chain length *vis-à-vis* that of the C-6 monolayers.

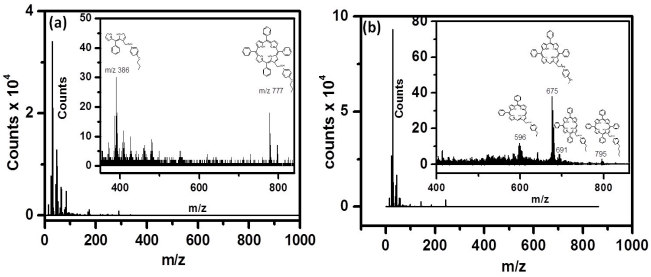

Fig. 4. SIMS of the monolayers of (a) **5a**; (b) **5b**, electro-grafted on Si (n^{++}) wafers.

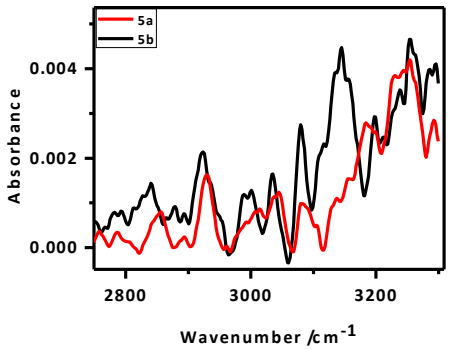

Fig. 5. FTIR spectra of the monolayers of **5a** and **5b**, electro-grafted on Si (n^{++}) wafers.

The IR peaks due to the -CH_2 vibrational modes can provide better insights about the van der Wall interactions between the alkylated porphyrin rings, parallely anchored on Si. This, in turn, may explain better packing of the **5b** monolayers *vis-à-vis* that of **5a**. In pure solid alkane monolayers, the hydrocarbon chains exist in an all-trans configuration such that the carbon backbone of each molecule lies in single planes. However, in liquid form, there is a substantial out-of-plane twisting about the individual bonds to alter the frequency of the -CH_2 vibrational modes.[45,49] The polarized FTIR spectrum (**Fig. 5**) of the **5a** monolayers exhibited N-H stretching frequency at 3251 cm^{-1} along with the symmetric (ν_s) and asymmetric stretching (ν_a) vibrational modes of the CH_2 groups at 2856 and 2927 cm^{-1} respectively. In contrast, the respective IR absorption peaks of the **5b** monolayers were at 3255, 2840 and 2921 cm^{-1}. Our results showed that the alkyl chains in the monolayers of **5b** are more rigid like that in pure solid alkanes, while that in the monolayers of **5a** are twisted. This clearly explained the observed better packing of the **5b** (C-11 linker) monolayers than the **5a** (C-6 linker) layers.[50] The X-ray photoelectron spectroscopy (XPS) peak of the monolayers at 99.5 eV accounted for the Si-C bond, while absence of the SiO_2 peak at 103 eV confirmed that monolayers were free of SiO_2 (**Fig. SL3**).

I-V MEASUREMENT

To measure the *I–V* characteristics, a metal/molecule/Si (n++) structure was completed (**Fig. 6(a)**), using a tiny drop of liquid

Hg (40 μm diameter) as the counter electrode. The area in contact with the grafted monolayer, measured using a goniometer was 0.002 mm^2.

The *I-V* curves (**Fig. 6(b)**) of the devices, constructed with the monolayers of **5a** and **5b** showed current rectification in the reverse bias. Maximum RR was observed at ±1 V with both the devices. Those, prepared using **5b** was very high (10^7), while that of **5a** (C-6 linker) was ~100. Nevertheless, both the systems were stable during repetitive voltage scanning upto 100 scans at a scan rate of 0.01V/s, but the RR reduced gradually from the original value to ~10000 for **5b** and to ~10 for **5a** after 50 scans.

It is already well known that when the electrodes are asymmetric (especially when the work functions of the electrode materials are different) any molecule can show current rectification.[51,52] Hence, to see the effect of asymmetric electrodes (if any), we also recorded the *I-V* curves of two control devices, made of (n++) Si/ Hg (**SL4 (a)**) and (n++) Si/C-11 alkyl monolayers/Hg (**SL4 (b)**). These showed marginal rectifications with RR I^+/I^- of 0.75 and 2 respectively. Recently, we have constructed the n^+-Si/pyrene C-11 monolayers/Hg device, which showed current rectification in the positive bias with RR of 100 at 1 V.[53] On the other hand, the n^+-Si/ 5-(4-undecenyloxyphenyl)-10,15,20triphenyl porphyrin (TPP C-11) monolayers /Hg system was constructed by our group showed a marginally asymmeteric *I-V* with significant hysteresis. In the positive bias scan (0 to +0.8 V), the current jumped by an order of magnitude at +0.6 V. However, on the reverse scan (+0.8 to 0 V) the current did not retrace the curve, and remained at a higher value.[54] Taken together, the *I-V* curves of all these devices clearly indicated that the results of the present devices are not because of electrode asymmetry. Moreover, the *I-V* results of the n^+-Si/TPP C-11 monolayers/Hg indicated that the observed rectifications in the negative bias with **5a**/**5b** molecules are not due to resonance tuneling through the TPP moiety.

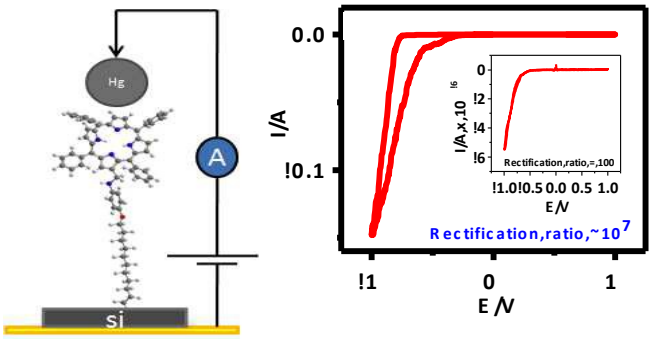

Fig. 6. (a) *I-V* measurement set up; **(b)** Experimental *I-V* characteristics of **5b** [**inset**: *I-V* curve of **5a**]. The *I-V* characteristics of all the samples were similar, and representative curves are shown.

Our AFM and fast scan CV results showed better molecular stacking of the **5b** monolayers, which may be due to the longer alkyl bridge in **5b** than in **5a**.[55] This may contribute to the better electrical characteristics of the **5b** monolayers, as the overlapping of electron clouds favours generation and transport of the charge carriers to induce intrinsic conductivity. Consequently, significantly higher maximum RR was observed with the **5b** monolayers. Control experiments, carried out with blank as well as C-11 alkyl chain-grafted Si-wafers showed nearly symmetrical sigmoidal *I-V* curves (**Fig. SL4.**), eliminating any doubt of artifacts.

The void sizes (~ 0.2–0.4 nm) of the present Si-alkylporphyrin/Hg junctions were too small compared to the size of the Hg drops (~ 40 μm). Hence, the Hg drops can't penetrate through the pinholes of the SAMs, and the measured *I-V* is expected to be direct. The statistical analyses of the data and junction yields are extremely valuable to discriminate artefacts from the real data. Earlier, Kim *et al.*,[56] and Nijhuis *et al.*,[57,58] employed extensive statistical analyses to assess the performance of their SAM-based devices. In the present work, we constructed only 80 devices with each of the compounds **5a** and **5b**. Nevertheless, we analyzed the statistics of our *I-V* results as shown in **Fig. 7** and **Table 1**, and summarized below. With compound **5a**, only 25% of the devices showed RR values 80-100, and an additional 15% devices showed RR 50-80. However, the RR values of 44% devices were <50, while 16% devices didn't show any rectification. The device statistics of the monolayers of compound **5b** was very impressive. The RR values of a majority (35%) of the devices were 10^5-10^6, while 21% of the devices showed RR values 10^6-10^7, 20% showed RR values 10^4-10^5, and the rest had RR values 1-10^4. The performances of the devices, made of the compounds **5a** and **5b** were satisfactory. In particular, the RR values of the Hg/**5b**/Si (n++) devices were far superior to that of the molecular rectifiers reported so far.[53,57,58]

Current rectification properties of various D-S-A-based SAMs and LB films, contacted by noble metal electrodes have been described.[59] Results of some of the representative examples clearly established significantly superior performance of the devices described in the present studies. For example, the LB film of a pyrenylcarbamate in a M-M-M junction showed a RR value of 130 at ~2.5 V.[60] Likewise, quinolinium and tetrahydroisoquinolinium iodides-based SAMs, deposited on Au substrates showed RR values of 50-150 and 30–80 respectively at ±1 V.[61,62] On the other hand, the RR value of SAMs of quinolinium salts joined by a truncated S–C_3H_6 group on Au surface was found to be 12 at ±1 V.[63] In another study, the LB monolayer of the D^+-π-A^- molecule, hexadecylquinolinium tricyanoquinodimethanide on Au electrodes showed maximum RR of 27.5 at 2.2 V.[64]

Table 1. Statistics of *I-V* data

Molecules	No. of samples	No. of devices in each sample	Total no. of devices	No. of devices exhibiting rectification
5a	10	8	80	67
5b	10	8	80	80

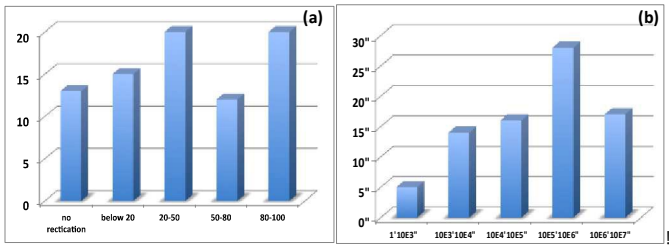

Fig. 7. Statistics of RR values of devices made with (a) **5a**; (b) **5b**.

However, literature reports on metal-porphyrin-semiconductor junctions are scarce. The SAMs of 4-aminothiophenol/ZnTPP/fulleropyrrolidine (PyC_2C_{60}) on Au (111) surface showed a modest RR of 24 at 1.8 V.[35]

Interestingly, self-assembled layers of Fe(III) 5,15-di[4-(s-acetylthio)phenyl]-10,20-diphenyl porphrin on annealed Au crystal facets on glass substrates showed asymmetric *I-V* curves with the highest RR up to 9000, but majority of the devices showed RR = 20 – 200 at ±1 V.[65]

To confirm our current rectification results, we computed the theoretical *I-V* curve of the device made of **5b**. Initially the ground state (GS) geometry of the molecule **5b** was optimized using *ab-initio* molecular orbital theory based LCAO-MO approach as implemented in the GAMESS software. The ionic optimization of molecule **5b** was carried out without any symmetry constraint at the B3LYP/6-31G (d,p) level of theory. For calculating the transport characteristics, a suitable device was constructed using the optimized configuration of the molecule as the central device region between two electrodes. Besides the active parts of the device, the central region also included sufficient parts of the contacts, such that the properties of the electrode regions can be described as bulk materials. This can be ensured by extending the central region into a few layers of the metallic contacts. The calculation of the electron-transport properties of the system was divided into two parts: (i) a self-consistent calculation for the electrodes with periodic boundary conditions in the transport direction, and (ii) a self-consistent open boundary calculation of the properties of the central region, where the electrodes define the boundary conditions. The complete details of the method is described in literature.[66]

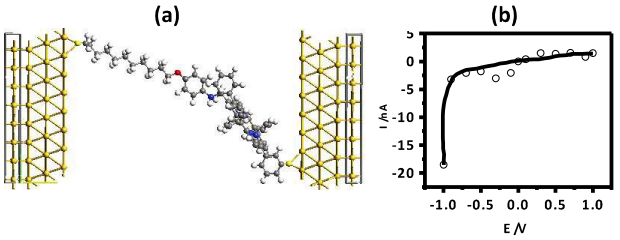

Figure 8. (a) Theoretical device geometry Au/ Molecule **5b**/Au. (b) Theoretical I-V

In the present experimental set-up, we have used highly doped Si substrate that is expected to undergo reconstruction. This restricted an accurate modelling of the molecule–substrate interface by the *ab-initio* formalisms using our computational resources. Hence, a model for a two-probe system was constructed (**Figure 8 (a)**) by placing the molecules between two Au electrodes. We modelled the electrodes as part of truncated solid crystals. Unlike Hg, which is liquid under the experimental conditions and has a complicated structure, Au possesses a well-defined face-centred cubic crystal structure. Also, the pseudo-potential for Au is robust and has been tested and used by many groups as a model electrode.[67,68] Understandably, the chosen system is not ideal to verify the experimental results. However, our calculation was primarily aimed at a qualitative understanding of the electron transport through these molecules, and not to make quantitative comparison, justifying our choice of Au electrodes. It is worth noting that recently Zheng et al.[69] reported the NDR property in C_{60} based electronic devices, wherein they claimed that the findings are independent of the type of electrodes used. For construction of the theoretical device, a thiol end group was used for attachment of the molecule with the electrode. The interface geometry of the thiol-terminated molecule and the electrode was optimized to ensure good overlap between the device and the electrodes.

Previously, we have reported the interaction of methyl thiol, a prototype device molecule, with an extended Au(111) surface using plane wave based pseudopotential method.[70] The result showed that the terminal S atom binds at the hollow site of the Au(111) surface and the distance between Au and S atoms is 2.52 A. Using this information, we constructed the model for our present calculation. Two Au(111)-8X8 surfaces were used as the left and right electrodes. The Au/molecule/Au configuration was divided into three parts: left electrode, right electrode, and the central scattering region. In our models, there were three Au layers in each of the left and right electrode unit cells. The scattering region was composed of the isolated molecule together with the respective two Au layers on the left and right sides. The electron-transport properties of the Au/molecule/Au systems were investigated using the ATK 11.2.3 program, where a semi-empirical extended Huckel theory in combination with the first-principle NEGF was employed.[71] A k-point sampling of 100 was used in the electron-transport direction (Z direction).[70] Consistent with the experimental results, the theoretical *I-V* also showed rectification in reverse bias (**Fig. 8(b)**).

Table 2. Energy levels for Tetra phenyl porphyrin, *p*-amino phenol and 5b

	Energy values in eV		
	Tetra phenyl porphyrin	*p*-amino phenol	**5b**
HOMO-2	-6.53074	-7.97294	-5.4757
HOMO-1	-5.52391	-7.04775	-5.1448
HOMO	-5.30622	-5.41507	-4.7990
LUMO	-2.55787	-0.48981	-2.1984
LUMO+1	-2.53066	-0.05442	-2.1739
LUMO+2	-0.9524	0	-0.5831

In general, the forward bias current-flow should be determined by the HOMO states of the molecules, while their respective LUMO states would dictate the reverse bias current. The observed rectification in the reverse bias is a result of alignment of the LUMO levels of the molecules with the Fermi-levels of the electrodes. To verify this, we determined the HOMO and LUMO energy levels (**Table 2.**) of **5b** by theoretical calculations using *ab-initio* method (GAMESS software). Ionic optimization without any symmetry constraint was carried out at the B3LYP/6-31G (d,p) level of theory where the exchange correlation functions are expressed using hybrid density functional theory. It was observed that HOMO of the molecule is at -4.707 eV and LUMO at -2.062 eV. Although, the HOMO of the molecule (located at p-amino phenol group) is in close proximity with Fermi level of electrode, but due to non contact with electrode resonance tunnelling will be difficult and for LUMO, the energy difference with the electrode Fermi level is large to undergo resonance tunnelling. Hence, the observed current rectification is unlikely to be due to resonant tunnelling but molecular asymmetry (D-s-A) favours Aviram and Ratner's mechanism for rectification.

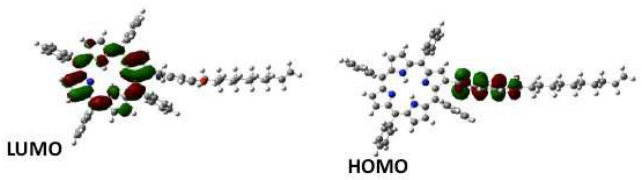

Fig. 9. Spatial distribution of the HOMO and LUMO energy levels of **5b**

From the spatial distribution of the HOMO and LUMO energy levels (**Fig. 9**), it was seen that the HOMO is localized on the *p*-aminophenol segment, while the LUMO is on the porphyrin ring, and their separation by the spacer CH_2 allowed unidirectional flow of electrons. This is consistent with the Aviram and Ratner theory that suggested that a single molecule with donor-spacer-acceptor (D-s-A) structure would behave as a diode when placed between two electrodes if a non-conjugated σ-bond bridge prevents direct overlap of the donor and acceptor energy levels. Moreover, a monolayer will rectify if its molecules are aligned in register between two electrodes so that they work together when electrons flow from electrode MD (attached to acceptor) to D, and exit from A to electrode MA (attached to donor).

To underscore the mechanism of electron flow between the donor and acceptor moieties, we also calculated the energy levels of the individual components (*p*-aminophenol and TPP) of **5b** using the same computational approach. The energy level diagram of the constituent species is shown in **Fig. 10**. The LUMO energy level of *p*-aminophenol was at a higher energy than the TPP moiety. This will make it as the donor. Thus, under reverse bias, when electrons flow from MD to D, the electrons will move from the HOMO of *p*-aminophenol to its LUMO, tunnel through the bridge to the vacant LUMO of TPP, and finally to the Hg electrode to complete the reverse-direction flow.

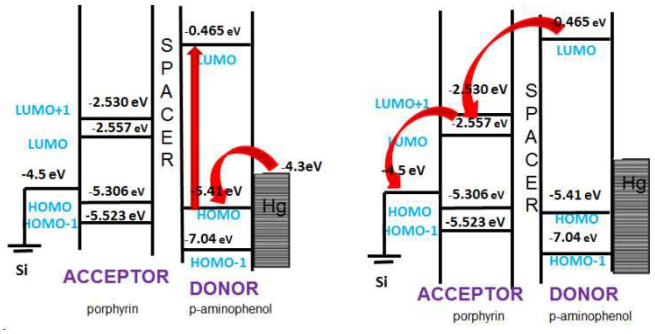

Fig. 10. Mechanism of rectification of devices made with **5b**.

In principle, reversing the orientation of the molecular dipole would change the *I-V* curves of the devices. This would also confirm that the observed rectification is not simply because of the non-symmetricity of the device system.[72] However, construction of this type of device is synthetically more demanding for the following reasons. The synthesis has to start with a unsymmetrical porphyrin wherein the phorphyrin needs to have the alkenyl attachment at one of its pyrrole moieties for its grafting to the Si wafers. Synthesis of the required phorphyrin proceeds via mono-bromination of porphyrin followed by Stile coupling with 11-trimethylstannyl undecene. Next, the unsymmetrical phorphyrin needs to be formylated for the subsequent attachment of the aniline moiety. However, formylation of unsymmetrical phorphyrins is never clean, and we experienced formation of a mixture of products, formylated at different sites and their purification was extremely cumbersome. Moreover, grafting such a molecule may not self-assemble in a similar manner as that used in the present work. Thus, the *I-V* results of the newly constructed device may provide unreliable results, despite having the reverse geometry. To confirm the hypothesis, the GS geometry of a **5b**-congener having the alkenyl attachment at one of the pyrrole moieties in the phorphyrin core was theoretically optimized, as done for **5b**. The GS geometry of the congener revealed that both the phorphyrin and aniline moieties lie on same side **(Fig. SL5.)**. So the Si- grafted **5b**-congener would be positioned in such a manner that the Hg electrode would preferably interact with the phorphyrin core. However, **5b** many have possible conformers, and the possibility of touching the mercury electrode by one of its straight conformers cannot be excluded. Nevertheless, based on the *I-V* results of the TPP C-11 monolayers[54] and that of **5a/5b**, it is tempting to propose that the observed current rectification is because of the nature of the molecules.

Experimental Section

General

EXPERIMENTAL DETAILS. Synthesis: All reagents and solvents (Sigma-Aldrich and Fluka) were of synthetic grade. Propionic acid, pyrrole, benzaldehyde, 4-nitrophenol was used after crystallisation. All solvents were dried and distilled before use. Tetrahydrofuran (THF) and hexane were distilled over Na under argon. DMF was dried with CaH_2 and distilled under vacuum. The ^{1}H NMR and ^{13}C NMR spectra were recorded with 200/300/500 (50/75/100) MHz spectrometers using deuterated solvents as the internal standards. The mass spectrometry was carried out with a MSMS (410 Prostar Binary LC with 500 MS IT PDA Detectors, Varian Inc, USA) and MALDI-TOF/TOF (BrukerUltraflex II) data systems. The IR spectra were recorded as films with a Jasco model A-202 FT-IR spectrometer and only the pertinent bands are expressed.

Synthesis

5,10,15,20-tetraphenylporphyrin ***1***. To a refluxing solution of benzaldehyde (5.30 g, 50 mmol) in propanoic acid was dropwise added pyrrole (3.35 g, 50 mmol) in propanoic acid. After refluxing for 2 h under stirring, the mixture was cooled to room temperature and kept for 12 h. The mixture was filtered, the precipitate washed with methanol, dried in vacuum, and column chromatographed (silica gel, 50% $CHCl_3$/hexane) to obtain **1** (1.62 g, 20%) after crystallization. purple crystals; m.p.: > 250 ^{o}C (MeOH/$CHCl_3$); δ_H(200 MHz; $CDCl_3$; Me_4Si) -2.78 (broad s, 2H), 8.84 (s, 8H), 8.21 (m, 8H), 7.76 (m, 12H); MALDI-TOF (HCCA matrix): m/z (%) 614 d.

5,10,15,20-tetraphenylporphyri-2-carbaldehyde ***2***.[38] To a refluxing and stirred solution of **1** (0.500 g, 0.814 mmol) in $CHCl_3$ (75 mL) was added $Cu(OAc)_2.H_2O$ (0.179 g, 0.895 mmol) in MeOH (12 mL). On completion of the reaction (*cf.* TLC, 30 min) the reaction mixture was brought to room temperature and triturated with MeOH to obtain the corresponding Cu(II)-porphyrinato acetate (0.647 g, ~quant.) as a purple powder. m.p.: >250 ^{o}C (MeOH/$CHCl_3$); UV-Vis (CH_2Cl_2): λmax [nm]: 302, 416, 540, 576, 617; MALDI-TOF: m/z (%): 795 d.

$POCl_3$ (7.9 mL, 52 mmol) was dropwise added to anhydrous DMF (5.5 mL, 75.6 mmol) at 0 ^{o}C to obtain the Vilsmeier complex as a thick golden liquid. To this was added a cold suspension of the Cu-porphyrinato salt (0.500 g, 0.73 mmol) in dicholoroethane (50 mL). The reaction mixture was brought to room temperature, refluxed for 5 h, cooled to room temperature, and left overnight. Concentrated H_2SO_4 (10 mL) was added to the ice-cold mixture, and stirring continued for 10 min. The green mixture was poured into ice-cold aqueous NaOH (0.625 M, 1 L) with occasional shaking till disappearance of the green colour. The mixture was extracted with $CHCl_3$ (2 × 200 mL), the organic layer washed with

saturated $NaHCO_3$ (2 × 350 mL) till neutral, and dried over $MgSO_4$. Solvent removal in vacuo followed by column chromatography (silica gel, 40% $CHCl_3$/hexane) of the residue gave **2** (0.085 g, 75%). mp: >250 °C (MeOH/$CHCl_3$); UV-Vis (CH_2Cl_2, nm): 431, 526, 567, 606, 664; δ_H (600 MHz; $CDCl_3$; Me_4Si) 9.40 (m, 1H), 9.24 (s, 1H), 8.90 (m, 4H), 8.78 (d, J = 2.3 Hz, 2H), 8.25 (d, J = 7.0 Hz, 2H), 8.20 (m, 6H), 7.79 (m, 12H); δ_C (75 MHz; $CDCl_3$; Me_4Si) 189.4, 142.5, 141.9, 141.7, 135.1, 134.7, 133.5, 130.8, 129.1, 128.5, 128.2, 128.0, 127.7, 127.5, 127.1, 126.9, 122.7, 120.7, 120.4, 120.1; MALDI-TOF: m/z (%) 642 d; LCMS m/z (%): 643.3 amu. Found: C 83.84; H, 4.82; N, 8.49. Calcd. for $C_{45}H_{30}N_4O$: C 84.09; H, 4.70; N, 8.72.

*4-(10-Undecenyloxy)-1-nitrobenzene **3a** and 4-(5-Hexenyloxy)-1-nitrobenzene **3b**.* A stirred mixture of 4-nitrophenol (0.500 g, 3.59 mmol), 10-undecenyl bromide (0.920 g, 3.95 mmol) or 5-hexenyl bromide (0.645 g 3.95 mmol) and K_2CO_3 (0.644 g, 5.14 mmol) in dry acetone was refluxed for 12 h. The reaction mixture was cooled, filtered over celite, concentrated, and residue dissolved in $CHCl_3$ (20 mL). The organic phase was washed with H_2O (2 × 20 mL) and brine (1 × 5 mL), and dried. Removal of solvent followed by column chromatography (silica gel, 2% EtOAc/hexane) of the residue furnished **3a** (1.0 g, 99%) and **3b** (0.791 g, 99%) as gels.

3a δ_H(600 MHz; $CDCl_3$; Me_4Si) 8.18 (m, 2H), 6.93 (m, 2H), 5.94 (m, 1H), 4.93 (m, 2H), 4.04 (t, J = 6.0 Hz, 2H), 2.04 (q, J = 6.0 Hz, 2H), 1.82 (quint, J = 6.6 Hz, 2H), 1.28 (m, 14H); δ_C (75 MHz; $CDCl_3$; Me_4Si) 164.3, 141.3, 139.2, 125.9, 114.4, 114.2, 68.9, 33.8, 29.5, 29.4, 29.3, 29.1, 29.0, 25.9; LCMS m/z (%): 292.0 amu. Found: C, 70.47; H, 8.78; N, 4.59. Calcd. for $C_{17}H_{25}NO_3$: C, 70.07; H, 8.65; N, 4.81.

3b: δ_H (600 MHz; $CDCl_3$; Me_4Si) 8.18 (m, 2H), 6.93 (m, 2H), 5.83 (m, 1H), 5.01 (m, 2H), 4.06 (t, J = 6.0 Hz, 2H), 2.14 (q, J = 6.0 Hz, 2H), 1.84 (quint, J = 6.8 Hz, 2H), 1.28 (m, 14H); δ_C (75 MHz; $CDCl_3$; Me_4Si) 164.2, 141.3, 138.3, 125.9, 115.0, 114.4, 68.7, 33.3, 28.4, 25.2; LCMS m/z (%): 222.0 amu. Found: C, 65.26; H, 6.77; N, 6.33. Calcd. for $C_{12}H_{15}NO_3$: C, 65.14; H, 6.83; N, 6.33.

*4-Undecenyloxyaniline (**4a**) and 4-Hexenyloxyaniline (**4b**)*. To a stirred mixture of **3a** or **3b** (0.684 mmol) and HCO_2NH_4 (0.068 g) in MeOH (5 mL), was added Zn dust (0.053.6 g, 0.82 mmol) under Ar. After 10 min, the mixture was filtered through celite and washed with Et_2O (2 × 20 mL), the organic layer washed with H_2O (2 × 15 mL) and brine (1 × 5 mL), and dried. Removal of solvent under vacuo afforded **4a** (0.162 g, 91%) and **4b** (0.116 g, 89%) as white powders. The samples turned brown very fast, hence were used for the next step without further purification.

*4-Undecenyloxyl-N-(5,10,15,20-tetraphenylporphyrin-2-ylmethyl)aniline (**5a**) and 4-Hexenyloxyl-N-(5,10,15,20-tetraphenylporphyrin-2-ylmethyl)aniline (**5b**).*[39] A mixture of **2** (0.075 g, 0.12 mmol), **4a** or **4b** (0.17 mmol), molecular sieves 4 Å (0.030 g) and AcOH (2 drops) in THF (5 mL) was refluxed till consumption of the starting materials (*cf.* 3 h). $NaBH_3CN$ (0.008 g, 0.15 mmol) in MeOH (5 mL) was added into the respective mixtures, which were refluxed for an additional 3 h. The mixtures were diluted with H_2O (5 mL) and extracted with $CHCl_3$ (50 mL). The organic layers were washed with H_2O (2 × 50 mL) and brine (1×5 mL), and dried. Removal of solvent under vacuo afforded the residues which on column chromatography (silica gel, 40% EtOAc/hexane) gave **5a** (0.080 g, 78%) as a solid and **5b** (0.075 g, 78 %) as a gel.

5a: mp: >250 °C; UV-Vis (CH_2Cl_2): λmax [nm] 411, 514, 548, 589, 646; δ_H (600 MHz; $CDCl_3$; Me_4Si) 8.70 (m, 6H), 8.64 (d, J = 5.9 Hz, 1H), 8.22 (m, 4H), 8.12 (m, 4H), 7.73 (m, 12H), 6.70 (m, 2H), 6.48 (d, J = 8.2 Hz, 2H), 5.81 (dd, J = 17.0, 10.0 Hz, 1H), 5.01 (d, J = 16.4 Hz, 1H), 4.95 (d, J = 10.6 Hz, 1H), 4.45 (broad s, 2H), 3.87 (t, J = 7.0 Hz, 2H), 3.74 (broad s, 1H), 2.11 (m, 2H), 1.74 (m, 2H), 1.54 (t, J = 8.2 Hz, 2H), 1.20-1.31 (m, 7H); δ_C (75 MHz; $CDCl_3$; Me_4Si) 151.8, 142.3, 142.2, 142.1, 141.9, 139.3, 134.72, 134.7, 134.7, 134.6, 133.2, 128.5, 127.8, 127.7, 127.3, 126.8, 126.7, 117.4, 115.7, 115.6, 114.7, 114.2, 68.8, 68.7, 33.9, 32.0, 29.8, 29.7, 29.6, 29.5, 29.2, 29.0, 26.1, 22.8, 22.2; MALDI-TOF m/z (%): 888 d. Found: C, 83.40; H, 6.17; N, 8.63. Calcd. for $C_{62}H_{57}N_5O$: C, 83.84; H, 6.47; N, 8.56.

5b: UV-Vis (CH_2Cl_2): λmax [nm] 410, 514, 549, 589, 645; δ_H (300 MHz; $CDCl_3$; Me_4Si) 8.82 (m, 6H), 8.64 (d, J = 4.8 Hz, 1H), 8.17 (m, 8H), 7.73 (m, 13H), 6.72 (m, 2H), 6.48 (m, 2H), 5.83 (m, 1H), 4.98 (m, 2H), 4.45 (s, 2H), 3.88 (t, J = 6.6 Hz, 1H), 1.97-2.19 (m, 3H), 1.76 (m, 3H), 1.54 (dt, J = 15.3, 7.6 Hz, 5H), 1.49 (broad s, 1H), 1.25 (m, 6H), -2.77 (broad s, 1H); δ_C (75 MHz; $CDCl_3$; Me_4Si) 151.7, 142.4, 142.3, 142.3, 142.1, 141.9, 138.7, 134.7, 134.6, 133.2, 128.5, 127.8, 127.7, 127.3, 126.8, 126.7, 120.7, 120.3, 119.5, 119.4, 115.7, 114.7, 68.6, 45.1, 33.6, 29.8, 29.0, 25.4; MALDI-TOF: m/z (%): 818 d. Found: C, 83.04; H, 6.08; N, 8.04. Calcd. for $C_{57}H_{47}N_5O$: C, 83.69; H, 5.79; N, 8.56; O, 1.96.

CHARACTERIZATION OF MONOLAYERS. The monolayers were characterized in terms of thickness, using an ellipsometer (Sentech: model SE400 adv); surface morphology by AFM imaging (Multiview 4000, Nanonics), de-ionized water contact angle (Data Physics System, model: OCA20), FT-IR (Bruker, 3000 Hyperion Microscope with Vertex 80 FTIR System, LN-MCT 315-025 detector) in polarized ATR mode (20 × objective) at an angle of 45° for 500 scans and the data were background corrected with freshly prepared Si-H monolayers, and molecular mass by SIMS (BARC make, Kore's Technology software) keeping Si-H as the reference. The XPS analysis of the deposited films was carried out using a Mg Kα (1253.6 eV) source and a MAC-2 electron analyzer. The XPS analysis chamber was maintained at a base vacuum of 10^{-9} mbar. The XPS binding energy scale was calibrated to Au $4f_{7/2}$ line at 83.95 eV.

PREPARATION OF H-TERMINATED SI WAFERS. N-type silicon wafers (orientation: 111; resistivity: 0.001-0.005 Ωcm) and 40% NH_4F were purchased from Siltronix and Fluka, respectively. The Si (111) wafers, cut into small pieces (~ 0.5 cm × 1.5 cm) were cleaned by heating in 3:1 (v/v) of conc. H_2SO_4 : 30% H_2O_2 (piranha) for 10 min at 80 °C. The wafers were washed with excess H_2O and immersed successively in a deaerated (purged with Ar for 30 min) 40% aqueous NH_4F for 10 min and 2% aqueous HF for 2 min. The wafers were washed with deionized H_2O for 1 min, dried under a stream of N_2 and immediately taken into the electrochemical cell for electro-grafting.

MONOLAYER FORMATION. The electrochemical deposition of **5a** and **5b** was carried out by cyclic voltammetry (CV) with a potentiostat/galvanostat system (model: Autolab PGSTAT 30) using the Si wafers as the working electrode (WE), Pt as the counter electrode (CE) and Ag/AgCl as the reference electrode (RE). The solution contained 0.1 M Bu_4NP as the electrolyte and **5a** or **5b** (1 μM) in dry CH_2Cl_2. The CV was run from 0 to -1 V for 30 cycles at 0.05 V/s scan rate under an inert

atmosphere. After the CV scans, the WE was sonicated in CH_2Cl_2 for 10 min to remove the electrolyte and the unreacted or physisorbed **5a** or **5b**. The WE was further washed with acetone, isopropanol and methanol to obtain the respective grafted monolayers.

JUNCTION AND MEASUREMENT SETUP. To measure the I–V characteristics, a metal/molecule/Si (n++) structure was completed by using a tiny drop of liquid mercury of diameter 40 ± 2 μm as the counter electrode. The contact area in the grafted monolayer was 0.002 mm^2. The I–V curves were recorded at room temperature in a dark box using a pAmeter–dc voltage source (HP 4140).

THEORETICAL CALCULATIONS. The ground state geometry optimization and molecular orbitals calculations of the molecule **5b**, TPP, *p*-aminophenol and **5b** congener were carried out using ab-initio molecular orbital theory based LCAO-MO approach as implemented in the GAMESS software. The ionic optimization of the molecules was carried out without any symmetry constraint at the B3LYP/6-31G (d,p) level of theory.

Conclusions

Overall, we have synthesized two porphyrin-based D-s-A prototype systems (**5a** and **5b**) with two alkenylated anilines, differing in the chain lengths of the alkenyl C-6 and C-11 respectively. These were individually electro-grafted on H-terminated Si surfaces to form monolayers. The *I–V* characteristics of the monolayers revealed pronounced, stable and reversible current rectification at room temperature in the negative bias. To the best of our knowledge such high RR values are rare except for some devices constructed by C. A. Nijhuis and Whitesides's group,[51,57,58] L. Venkataraman[52] and a recent publication from our own group.[53] The monolayer with the C-11 linker was more compact and showed a 10^5 times high rectification ratio (RR) relative to the other similar system having the C-6 linker possibly because of compact packing. The rectification mechanism was explained on the basis of Aviram and Ratner theory of rectification by using *ab-initio* molecular orbital calculations.

Notes and references

[a]*Dr. Kavita Garg, Prof. Sandip K. Nayak, Prof. SubrataChattopadhyay, Bio-Organic Division, Bhabha Atomic Research Centre, Mumbai, India*
Email: kavitachemistry1@gmail.com, schatt@barc.gov
[b]*Dr. Chiranjib Majumder, Chemistry Division, Bhabha Atomic Research Centre, Mumbai, India*
[c]*Prof. Dinesh K. Aswal, Prof. Shiv K. Gupta, Chemistry Division, Bhabha Atomic Research Centre, Mumbai, India*

† Electronic Supplementary Information (ESI) available: Schematic representation of electrografting mechanism, Electrochemical deposition of undecene, I-V characteristics of blank and C-11 alkyl monolayer on silicon wafer, XPS of monolayer and optimised geometry of **5b**-congener with reverse geometry. Tables of atom coordinates and absolute energies used for theoretical calculations. These materials are available free of charge. See DOI: 10.1039/b000000x/

1 A. Aviram and M. Ratner, *Chem. Phys. Lett.*, 1974, **29**, 277–283.
2 M. A. Reed, *Science.*, 1997, **278**, 252–254.
3 R. F. Service, *Science*, 2001, **294**, 2442–2443.
4 Z. J. Donhauser, B. A. Mantooth, K. F. Kelly, L. A. Bumm, J. D. Monnell, J. J. Stapleton, D. W. Price Jr., A. M. Rawlett, D. L. Allara, J. M. Tour and P. S. Weiss, *Science*, 2001, **292**, 2303–2307.
5 M. Brink, *Nature*, 2002, **417**, 725–729.
6 R. M. Metzger, J. W. Baldwin, W. J. Shumate, I. R. Peterson, P. Mani, G. J. Mankey, T. Morris, G. Szulczewski, S. Bosi, M. Prato, A. Comito and Y. Rubin, *J. Phys. Chem. B*, 2003, **107**, 1021–1027.
7 A. Honciuc, A. Jaiswal, A. Gong, K. Ashworth, C. W. Spangler, I. R. Peterson, L. R. Dalton and R. M. Metzger, *J. Phys. Chem. B*, 2005, **109**, 857–871.
8 R. M. Metzger, B. Chen, U. Höpfner, M. V. Lakshmikantham, D. Vuillaume, T. Kawai, X. Wu, H. Tachibana, T. V. Hughes, H. Sakurai, J. W. Baldwin, C. Hosch, M. P. Cava, L. Brehmer and G. J. Ashwell, *J. Am. Chem. Soc.*, 1997, **119**, 10455–10466.
9 T. Xu, I. R. Peterson, M. V. Lakshmikantham and R. M. Metzger, *Angew. Chemie - Int. Ed.*, 2001, **40**, 1749–1752.
10 J. W. Baldwin, R. R. Amaresh, I. R. Peterson, W. J. Shumate, M. P. Cava, M. a. Amiri, R. Hamilton, G. J. Ashwell and R. M. Metzger, *J. Phys. Chem. B*, 2002, **106**, 12158–12164.
11 J. M. Buriak, *Chem. Rev.*, 2002, **102**, 1271–1308.
12 W. Davis, W. Svec, M. Ratner and M. Wasielewski, *Nature*, 1998, **396**, 60–63.
13 R. M. Metzger, *Acc. Chem. Res.*, 1999, **32**, 950–957.
14 C. Joachim, J. K. Gimzewski and A. Aviram, *Nature*, 2000, **408**, 541–8.
15 G. J. Ashwell and D. S. Gandolfo, *J. Mater. Chem.*, 2001, **11**, 246–248.
16 F. Schreiber, *Prog. Surf. Sci.*, 2000, **65**, 151–256.
17 S. Ciampi, J. B. Harper and J. J. Gooding, *Chem. Soc. Rev.*, 2010, **39**, 2158–2183.
18 H. Haick and D. Cahen, *Acc. Chem. Res.*, 2008, **41**, 359–366.
19 A. Vilan, O. Yaffe, A. Biller, A. Salomon, A. Kahn and D. Cahen, *Adv. Mater.*, 2010, **22**, 140–159.
20 A. B. Sieval, A L. Demirel, J. W. M. Nissink, M. R. Linford, J. H. Van Der Maas, W. H. D. Jeu, H. Zuilhof and E. J. R. Sudhölter, *Langmuir*, 1998, **14**, 1759–1768.
21 J. Terry, M. R. Linford, C. Wigren, R. Cao, P. Pianetta and C. E. D. Chidsey, *Appl. Phys. Lett.*, 1997, **71**, 1056.
22 M. P. Stewart and J. M. Buriak, *Angew. Chem. Int. Ed.*, 1998, **37**, 3257–3260.
23 M. R. Linford, P. Fenter, P. M. Eisenberger and C. E. D. Chidsey, *J. Am. Chem. Soc.*, 1995, **117**, 3145–3155.
24 J. Buriak and M. Allen, *J. Am. Chem. Soc.*, 1998, **7863**, 1339–1340.
25 A. Bansal, X. Li, I. Lauermann and N. S. Lewis, *J. Am. Chem. Soc.*, 1996, **118**, 7225–7226.
26 D. K. Aswal, S. P. Koiry, B. Jousselme, S. K. Gupta, S. Palacin and J. V. Yakhmi, *Phys. E*, 2009, **41**, 325–344.
27 M. Jurow, A. E. Schuckman, J. D. Batteas and C. M. Drain, *Coord. Chem. Rev.*, 2010, **254**, 2297–2310.
28 L. Esaki, *Phys. Rev.*, 1958, 0–1.
29 H. Lawrence and G. Ralph, *Annu. Rev. Chem.*, 1992, **43**, 437–463.

30 K. M. Roth, N. Dontha, R. B. Dabke, D. T. Gryko, C. Clausen, J. S. Lindsey, D. F. Bocian and W. G. Kuhr, *J. Vac. Sci. Technol. B Microelectron. Nanom. Struct.*, 2000, **18**, 2359–2364.
31 D. Gryko, J. Li, J. R. Diers, K. M. Roth, D. F. Bocian, W. G. Kuhr and J. S. Lindsey, *J. Mater. Chem.*, 2001, **11**, 1162–1180.
32 K. M. Roth, J. S. Lindsey, D. F. Bocian and W. G. Kuhr, *Langmuir*, 2002, **18**, 4030–4040.
33 K. M. Roth, A. A. Yasseri, Z. Liu, R. B. Dabke, V. Malinovskii, K.-H. Schweikart, L. Yu, H. Tiznado, F. Zaera, J. S. Lindsey, W. G. Kuhr and D. F. Bocian, *J. Am. Chem. Soc.*, 2003, **125**, 505–17.
34 X. Lu, M. Li, C. Yang, L. Zhang, Y. Li, L. Jiang, H. Li, L. Jiang, C. Liu and W. Hu, *Langmuir*, 2006, **22**, 3035–3039.
35 F. Matino, V. Arima, M. Piacenza, F. Della Sala, G. Maruccio, R. J. Phaneuf, R. Del Sole, G. Mele, G. Vasapollo, G. Gigli, R. Cingolani and R. Rinaldi, *ChemPhysChem*, 2009, **10**, 2633–2641.
36 T. E. Mallouk and H. Lee, *J. Chem. Ed*.,1990, **67**, 829–834.
37 A. Giraudeau, H. J. Callot, J. Jordan, I. Ezhar and M. Grossz, *J. Am. Chem. Soc.*, 1979, **101**, 3857–3862.
38 H. K. Hombrecher, V. M. Gherdan, S. Ohm, J. a. S. Cavaleiro, M. Da Graça, P. M. S. Neves and M. De Fátima Condesso, *Tetrahedron*, 1993, **49**, 8569–8578.
39 E. E. Bonfantini, A. K. Burrell, W. M. Campbell, M. J. Crossley, J. J. Gosper, M. M. Harding, D. L. Officer and D. C. W. Reid, *J. Porphyr. Phthalocyanines*, 2002, **06**, 708–719.
40 C. Welch, S. J. Archibald and R. W. Boyle, *Synthesis*, 2009, 551–556.
41 L. Zhang, L. Li, S. Chen and S. Jiang, *Langmuir*, 2002, **18**, 5448–5456.
42 Y. J. Liu, N. M. Navasero and H. Z. Yu, *Langmuir*, 2004, **20**, 4039–4050.
43 J. K. Bal, S. Kundu and S. Hazra, *Chem. Phys. Lett.*, 2010, **500**, 90–95.
44 Y. Coffinier, G. Piret, M. R. Das and R. Boukherroub, *Comptes Rendus Chim.*, 2013, **16**, 65–72.
45 M. Perring, S. Dutta, S. Arafat, M. Mitchell, P. J. A. Kenis and N. B. Bowden, *Langmuir*, 2005, **21**, 10537–10544.
46 S. Lenfant, D. Guerin, F. Tran Van, C. Chevrot, S. Palacin, J. P. Bourgoin, O. Bouloussa, F. Rondelez and D. Vuillaume, *J. Phys. Chem. B*, 2006, **110**, 13947–13958.
47 X. Qian, Z. Tai, X. Sun, S. Xiao, H. Wu and Z. Lu, *Thin Solid Films*, 1996, **285**, 432–435.
48 W. R. Scheidt, *Acc. Chem. Res.*, 1977, **10**, 339–345.
49 R. L. Cicero, M. R. Linford and C. E. D. Chidsey, *Langmuir*, 2000, **16**, 5688–5695.
50 X. Qiu, C. Wang, Q. Zeng, B. Xu, S. Yin, H. Wang, S. Xu and C. Bai, *J. Am. Chem. Soc.*, 2000, **122**, 5550–5556.
51 L. Yuan, R. Breuer, L. Jiang, M. Schmittel, and C. A. Nijhuis *Nano Lett.,* 2015, **15**, 5506-5512
52 B. Capozzi, J. Xia, O. Adak, E. J. Dell, Z. Liu, J. C. Taylor, J. B. Neaton, L. M. Campos & L. Venkataraman *Nature Nanotechnology* 2015, **10**, 522–527.
53 K. Garg, C. Majumder, S. K. Nayak, D. K. Aswal, S. K. Gupta and S. Chattopadhyay, *Phys. Chem. Chem. Phys.*, 2015, **17**, 1891–1899.
54 S. P. Koiry, D. K. Aswal, A. K. Chauhan, V. Saxena, S. K. Nayak, S. K. Gupta and J. V. Yakhmi, *Chem. Phys. Lett.*, 2008, **453**, 68–72.
55 X. Wang, P. E. Colavita, K. M. Metz, J. E. Butler and R. J. Hamers, *Langmuir*, 2007, **23**, 11623–11630.
56 T. -W. Kim, G. Wang, H. Lee and T. Lee, *Nanotechnol*., 2007, **18**, 315204.
57 C. A. Nijhuis, W. F. Reus, J. R. Barber, M. D. Dickey and G. M. Whitesides, *Nano Lett.*, 2010, **10**, 3611–3619.
58 C. A. Nijhuis, W. F. Reus and G. M. Whitesides, *J. Am. Chem. Soc.*, 2009, **131**, 17814–17827.
59 G. J. Ashwell and A. Mohib, *J. Am. Chem. Soc*. 2005, **127**, 16238-16244.
60 A. C. Brady, B. Hodder, A. Scott Martin, J. Roy Sambles, C. P. Ewels, R. Jones, P. R. Briddon, A. M. Musa, C. A. Panetta and D. L. Mattern, *J. Mater. Chem*., 1999, **9**, 2271–2275.
61 G. J. Ashwell and A. Mohib, *J. Am. Chem. Soc*. 2005, **127**, 16238-16244.
62 G. J. Ashwell, A. Mohib, C. J. Collins and A. Aref, *Synth. Metals* 2009, **159**, 2282–2285.
63 G. J. Ashwell, W. D. Tyrrell and A. J. Whittam, *J. Mater. Chem*. 2003, **13**, 2855–2857.
64 R. M. Metzger, T. Xu and I. R. Peterson, *J. Phys. Chem. B* 2001, **105**, 7280–7290.
65 X. Wang, G.-C. Wang and K. M. Lewis, *Mat. Chem. Phys*. 2012, **136**, 190–195.
66 S. Datta, *Superlattices Microstruct.*, 2000, **28**, 253–278.
67 A. Nitzan and M. A. Ratner, *Science*, 2003, **300**, 1384–1389.
68 M. Di Ventra, S. T. Pantelides and N. D. Lang, *Phys. Rev. Lett*. 2000, **84**, 979.
69 X. Zheng, W. Lu, T. A. Abtew, V. Meunier and J. Bernholc, 2010, **4**, 7205–7210.
70 C. Majumder, H. Mizuseki and Y. Kawazoe, *J. Chem. Phys.*, 2003, **118**, 9809–9813.
71 K. Stokbro, D. E. Petersen, S. Smidstrup, A. Blom, M. Ipsen and K. Kaasbjerg, *Phys. Rev. B - Condens. Matter Mater. Phys.*, 2010, **82**, 1–7.
72 A. C. Brady, B. Hodder, A. S. Martin, J. R. Sambles, C. P. Ewels, R. Jones, P. R. Briddon, A. M. Musa, C. A. Panetta and D. L. Mattern, *J. Mater. Chem.*, 1999, **9**, 2271–2275